

# DENDRITIC PATTERN FORMATION AND CONTACT LINE FORCES DURING DEWETTING OF DILUTE POLYMER SOLUTIONS ON A HYDROPHOBIC SURFACE

Volfango Bertola <sup>1</sup> \*

<sup>1</sup> Laboratory of Technical Physics, School of Engineering, University of Liverpool, Brownlow Hill, Liverpool L69 3GH, United Kingdom; Volfango.Bertola@liverpool.ac.uk

**Abstract:** The micro-scale morphology of the receding contact line of dilute polyethylene oxide solution drops ( $c \sim 100$  ppm) after impact and inertial spreading on a fluorinated hydrophobic surface is investigated. One can observe the formation of transient liquid filaments and dendritic structures that evolve into a bead-on-a-string structure similar to the well-known capillary breakup mechanism of dilute polymer solutions, which confirm the interaction between stretched polymer coils and the receding three-phase contact line. The estimation of the average polymer force per unit contact line length provides a quantitative explanation for the reduction of the contact line retraction velocity reduction observed experimentally.

**Keywords:** Dilute polymer solution; Wetting; Contact line; Coil-stretch transition.

**PACS:** 47.55.D-, 47.50.-d, 47.80.Jk

**Citation:** Bertola, V. Dendritic pattern formation and contact line forces during dewetting of dilute polymer solutions on a hydrophobic surface. *Colloids Interfaces* **2021**, *1*, 0. <https://doi.org/>

Received:

Accepted:

Published:

**Publisher's Note:** MDPI stays neutral with regard to jurisdictional claims in published maps and institutional affiliations.

**Copyright:** © 2021 by the author. Submitted to *Colloids Interfaces* for possible open access publication under the terms and conditions of the Creative Commons Attribution (CC BY) license (<https://creativecommons.org/licenses/by/4.0/>).

## 1. Introduction

The wetting dynamics of complex fluids, such as polymer or surfactant solutions, can be significantly different with respect to simple liquids. Even in the case of very dilute solutions, the comparison with a Newtonian solvent (e.g. water) reveals significant differences in the behaviour of the moving contact line during the spreading and/or receding phase, in the amplitude of the apparent dynamic contact angle, and in the intrinsic time scale of the phenomenon. A well-known example is the dynamic wetting behaviour of dilute polymer solution droplets impacting on low-energy (hydrophobic) surfaces. When a droplet of water falls on to a hydrophobic surface, such as the waxy leaf of a plant, the drop is often observed to bounce off; however, for about 20 years it has been known that the addition of very small quantities ( $c \sim 100$  ppm) of a high-molecular weight flexible polymer such as poly-(ethylene oxide) (PEO) can completely prevent rebound, by reducing the recoil velocity of the drop after the inertial spreading of two orders of magnitude [1,2]. This is surprising since the shear viscosity and surface tension of such drops are almost identical to those of pure water.

This phenomenon was initially understood as a direct consequence of the nonlinear bulk rheology of the fluid, namely of the elongational viscosity, and normal stresses [1–3]. However, the interpretation in terms of bulk elongational viscosity was soon contradicted by a number of different experiments revealing the prevailing role of dynamic wetting [4–8]. Remarkably, some of the elongational viscosity measurements used to support the initial understanding of the phenomenon turned out to be highly inaccurate [9]. Later on, it was proposed to describe the contact line dynamics using a modified lubrication equation for thin films including an additional dissipative term proportional to the first normal stress coefficient [3]. This approach, however, does not consider the elastic force associated with normal stresses, which should accelerate drop retraction instead of slowing it down as observed experimentally. Moreover, in dilute solutions the magnitude of normal stresses is too small, therefore the effect on the contact

38 line dynamics is negligible; a significant reduction of the contact line velocity can be  
39 obtained only with normal stress values typical of semi-dilute solutions [9].

40 More recently, it was observed that when dilute solution drops are doped with  
41 fluorescent  $\lambda$ -DNA, the de-wetted substrate is covered with stretched DNA molecules,  
42 oriented in the direction perpendicular to the receding contact line [7]. Independent  
43 experiments on forced dewetting showed that polymer deposited on the substrate  
44 results into a velocity-dependent force at the contact line [10]. These results suggest  
45 that the receding contact line is slowed down by a force, in the direction opposed to the  
46 contact line movement, which arises in the liquid film left behind the drop edge during  
47 retraction.

48 Here, the microscopic contact line morphology during dewetting of dilute polymer  
49 solution drops impacting on a hydrophobic surface is studied by high-speed microscopy,  
50 to get a deeper understanding of the origin of contact line forces. Experiments reveal  
51 the formation of transient microscopic dendritic structures generated by the receding  
52 contact line, which evolve in a similar fashion to the well-known beads-on-a-string  
53 mechanism [11]. Fingering and/or dendritic structures on a moving contact line were  
54 observed during spreading of surfactant solutions [12], evaporation of aqueous polymer  
55 solutions [13] and particle-laden droplets [14], however they have never been observed  
56 during rapid dewetting following drop impact. It is demonstrated that the shear flow in  
57 the liquid wedge near the contact line induces a second order coil-stretch transition of  
58 the polymer molecules leading to a significant increase of the local viscosity [15], which  
59 enables a quantitative estimation of the contact line friction. The proposed approach  
60 is substantially different from most of the existing studies, which interpret the same  
61 phenomenon as a consequence of a hypothetical but unrealistic elongational flow within  
62 the impacting drop.

## 63 2. Materials and Methods

64 Polymer solutions were prepared by dissolving polyethylene oxide (PEO) with  
65 average molecular weight of 4,000 kDa (Sigma-Aldrich) in de-ionised water (Barnstead  
66 Easypure), at concentrations of 40, 60, 100 and 200 ppm. Since the overlap concentration  
67 of this polymer in water, calculated based on the Mark-Houwink correlation for the  
68 characteristic viscosity, is approximately 570 ppm [9,16,17], these solutions fall within the  
69 dilute regime. In this regime viscosity,  $\eta$ , and the relaxation time,  $\tau$ , are approximately a  
70 linear and a square root function of the polymer concentration, respectively [18]. Unlike  
71  $\eta$  and  $\tau$ , the surface tension,  $\sigma$ , of PEO solutions is approximately the same as the solvent  
72 ( $\sim 70$  mN/m) on the timescale of experiments [19].

73 The impact substrates were glass slides coated with Fluoropel PFC1302A (Cytonix  
74 Corp., USA), a 2% fluoropolymer solution in low boiling point (135°C) fluorosolvent,  
75 with equilibrium contact angle for water of  $105^\circ \pm 2^\circ$ ; the Fluoropel coating was created  
76 by dipping glass slides into the liquid, and then dried at 90°C for 10 minutes to optimize  
77 adhesion.

78 Drops were released from a blunt hypodermic needle (gauge 21, i.d. 0.495 mm)  
79 suspended above the target surface. The equilibrium drop diameter (obtained from drop  
80 mass measurements) was in the range between 2.92 mm and 3.06 mm for all fluids. The  
81 impact velocity was controlled by adjusting the falling height between 20mm and 140  
82 mm, corresponding to impact Weber numbers between 13 and 110; the Weber number,  
83  $We = \rho v_z^2 D_0 / \sigma$ , where  $\rho$  is the fluid density,  $v_z$  denotes the vertical impact velocity,  
84 and  $D_0$  denotes the equilibrium drop diameter prior to impact, is routinely used in the  
85 drop impact literature to characterise impacts through the competition between inertial  
86 and capillary forces, although it does not take into account the viscous dissipation. To  
87 account for viscous effects, one can introduce the Reynolds number  $Re = \rho v_z D_0 / \mu$ ,  
88 where  $\mu$  is the fluid viscosity, representing the ratio of inertial to viscous forces, and the  
89 Ohnesorge number  $Oh = \sqrt{We} / Re$ , representing the ratio of viscous to capillary forces.

90 The contact line details during drop impact and recoil were recorded using a high-  
91 speed CMOS camera (Phantom v9.1) equipped with a Keyence VH-100ZR zoom lens  
92 (magnification range of 100x-1000x), at the speed of 5,000 fps and a resolution of 480x480  
93 pixels, corresponding to  $1.46 \mu\text{m}/\text{pixel}$ ; the camera and the lens were arranged vertically  
94 looking at the substrate from below, while illumination was provided by an optic fiber  
95 halogen illuminator (ThorLabs).

### 96 3. Results

#### 97 3.1. Contact line morphology

98 The microscopic contact line morphology during drop retraction on a hydropho-  
99 bized glass substrate for different concentrations of PEO and impact Weber number  
100  $We \approx 110$  is displayed in Figure 1, and compared with the contact line of a drop of pure  
101 water in the same experimental conditions. While the contact line of the water appears  
102 almost perfectly smooth, the contact line of the polymer solution drop exhibits large local  
103 deformations, and leaves behind microscopic liquid filaments as it sweeps the surface.  
104 Filaments are distributed uniformly around the contact line, and their width ranges  
105 between approximately  $2\mu\text{m}$  and  $30\mu\text{m}$ . The structure and density of these filaments  
106 depends on the polymer concentration in the fluid: for  $c < 100$  ppm, one can observe  
107 linear filaments oriented in the radial direction, their density being increased with the  
108 polymer concentration; for  $c \gtrsim 100$  ppm, there are less but thicker filaments, displaying  
109 numerous dendritic ramifications.

110 Filaments evolve displaying a pseudo capillary instability mechanism, until they  
111 locally break up into secondary microscopic droplets, in a similar fashion to the well-  
112 known bead-on-a-string capillary breakup mechanism characteristic of many viscoelastic  
113 fluids [11]. It is important to remark, however, that such resemblance is only visual,  
114 because while in conventional capillary breakup the flow in the liquid filament is purely  
115 elongational [20,21], the filaments observed in the present experiments are in contact  
116 with a solid surface, therefore they are in shear flow. On the reverse of the coin, the  
117 appearance of a bead-on-a-string breakup dynamics suggests that polymer stretching  
118 does occur also in shear flow, as predicted theoretically by de Gennes [15]. At higher  
119 polymer concentrations, filaments are more stable therefore the breakup mechanism is  
120 less noticeable on the timescale of the experiment.

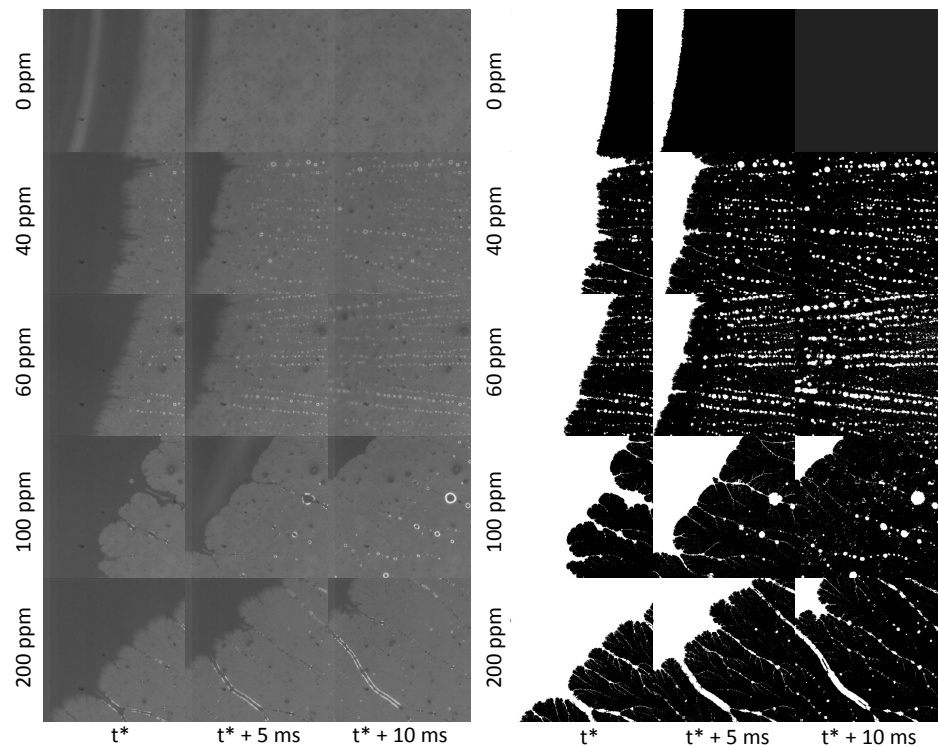


**Figure 1.** Microscopic contact line morphology during drop retraction on a hydrophobized glass substrate for different concentrations of PEO and impact Weber number  $We \approx 110$ . Left panel: raw images; right panel: the same images enhanced by background subtraction, histogram equalization and conversion to binary. Each frame has a size of  $700 \mu\text{m}$ . See original videos in supplementary material.

121 This complex morphology, which can be observed only at the microscale, suggests  
 122 that even from the macroscopic point of view the term *contact line* is not appropriate to  
 123 indicate the drop edge, but one should rather use the expression *apparent contact line*,  
 124 similar to the convention used for contact angles.

### 125 3.2. Estimation of the polymer elastic force in a liquid wedge

126 The hydrodynamics of the liquid wedge near the contact line can be modelled as the  
 127 flow between a fixed horizontal surface (the substrate) and a plate inclined at an angle  
 128  $\theta$  (corresponding to the instantaneous value of the apparent dynamic contact angle),  
 129 moving at velocity  $U$ , as shown schematically in Figure 2a. The minimum thickness of  
 130 the liquid film,  $h_0$ , must be no less than the unperturbed size of the polymer coils,  $R_0$ ; for  
 131 PEO molecules in water, one finds  $R_0 = 0.0888M^{0.5} = 178\text{nm}$ , where  $M$  is the molecular  
 132 weight [22], hence one can take an order of magnitude  $h_0 \approx 0.2\mu\text{m}$ . Polymer coils  
 133 are subject to hydrodynamic interaction with the solvent, with a characteristic Zimm  
 134 time  $\tau_0 \approx 0.2\eta_s R_0^3 / k_B T = 0.27\text{ms}$ , and a Rouse time  $\tau_R \approx 2R_h \eta_s R_0^2 / \pi k_B T = 0.41\text{ms}$ ,  
 135 where  $\eta_s$  is the solvent viscosity,  $k_B$  is Boltzmann's constant,  $T$  is temperature, and  
 136  $R_h = 0.0145M^{0.57} = 84\text{nm}$  is the radius of gyration.

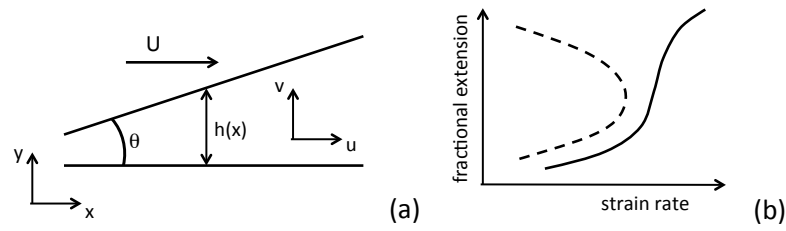


**Figure 2.** (a) Schematic of the liquid wedge near the contact line and (b) schematic of supercritical coil-stretch transition [15].

137 In a reference frame originating on the contact point, the velocity components  
 138 parallel and perpendicular to the substrate during drop retraction are, respectively,  
 139  $u \approx Uy/h(x)$  and  $v \approx \zeta(\theta)x$ , where  $h(x) \approx \theta x$  is the liquid film thickness and  $\zeta(\theta)$  is  
 140 a positive function of the apparent contact angle. The velocity gradient of this flow  
 141 field can be split into its symmetrical part,  $A = \frac{1}{2}(u_y + v_x) = \frac{1}{2}(U/h + \zeta)$ , associated  
 142 with a pure deformation, and its anti-symmetrical part  $\omega = \frac{1}{2}(u_y - v_x) = \frac{1}{2}(U/h - \zeta)$ ,  
 143 associated with a pure rotation. Since  $\zeta(\theta) > 0$ ,  $\omega/A < 1$  therefore it is possible to  
 144 have strong distortions of the polymer coils, even in the absence of elongational flow  
 145 [15,23]. This corresponds to a second-order transition from coil to stretch conformation  
 146 state, where the end-to-end distance of the polymer chain increases monotonously but  
 147 steeply (i.e., with a constantly positive slope of the stretching ratio,  $l = r/L$ , where  $r$  is  
 148 the polymer elongation and  $L$  the length of the fully stretched chain), with respect to the  
 149 control parameter  $\zeta(\theta)$  (i.e.,  $dl/d\zeta > 0$ ) [15]. Such transition, illustrated schematically  
 150 in Figure 2b, is reversible and, unlike the first-order coil-stretch transition occurring in  
 151 purely elongational flows, does not exhibit hysteresis.

For the two-dimensional steady-state shear flow introduced above, and following  
 the classical finite extensibility approach [24], de Gennes obtained the following implicit  
 relationship between the stretching ratio and the velocity gradient [15]:

$$l = \frac{3}{Z\mathcal{L}^{-1}(l)} \left\{ 1 + \frac{1}{6} \frac{\left(\frac{U}{h} + \zeta\right)^2 \tau^2}{\frac{[\mathcal{L}^{-1}(l)]^2}{9l^2} - \frac{U}{h} \zeta \tau^2} \right\} \quad (1)$$

where  $Z$  is the number of monomers in one polymer chain,  $\tau$  is the relaxation time,  $\tau(l) \approx \tau_R/(1 + 1/l)$ , and  $\mathcal{L}^{-1}(l)$  is the inverse Langevin function, which can be estimated for example using Kroger's approximation [25]:

$$\mathcal{L}^{-1}(l) = \frac{3l - (l/5)(6l^2 + l^4 - 2l^6)}{1 - l^2} \quad (2)$$

The stretching ratio obtained from Eq. (1) can be used to calculate the recall entropic force of a stretched polymer coil. In the dumbbell model, where the chain is represented by one single spring of fractional extension  $l = r/L$ , the restoring force is written as [15,24]:

$$F = \frac{k_B T L}{R_0^2} \mathcal{L}^{-1}(l) \quad (3)$$

#### 152 4. Discussion

153 To understand how the theoretical framework outlined in Section 3.2 above can be  
 154 applied to the case of the receding contact line of a polymer solution drop after impacting  
 155 onto a solid surface, one must observe the drop dynamics at the very beginning of the  
 156 recoil stage after maximum spreading. Figure 3a shows that at the beginning of recoil  
 157 the contact line moves very slowly (although it is not pinned on the surface) compared to  
 158 the displacement of the liquid free surface that defines the apparent contact angle, and

159 causes the liquid in the rim, visible from the top views displayed in Figure 3b, to flow back  
 160 towards the centre of the drop. Previous works [7–9] show that while in water drops the  
 161 fluid velocity is the same as the velocity of the receding contact line, in dilute polymer  
 162 solution drops the bulk velocity of the fluid during retraction is two or three orders  
 163 of magnitude larger than the contact line velocity. In particular, particle velocimetry  
 164 measurements of the radial velocity in the lamella of a 200 ppm polyethylene oxide  
 165 solution drop during retraction show the recoil velocity is approximately 300 mm/s, and  
 166 grows linearly from the centre to the rim [8].

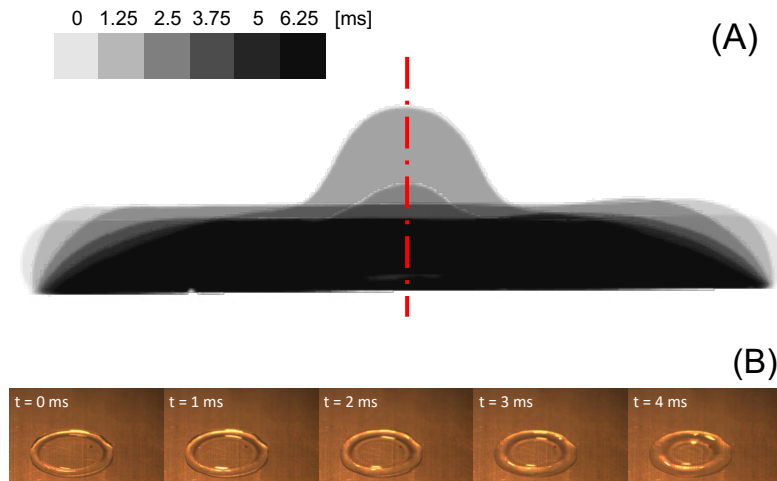


**Figure 3.** (a) Stroboscopic side view of a PEO aqueous solution drop ( $D_0 \approx 3$  mm) impacting on a PTFE surface at the beginning of recoil after maximum spreading ( $c = 200$  ppm;  $We = 45$ ;  $D_{max}/D_0 \approx 2.2$ ). The gray levels in region near the contact line correspond to the time since maximum spreading. (b) Top view of the same drop showing the toroidal rim during the first 4 ms of recoil after maximum spreading.

The drop dynamics illustrated in Figure 3 suggests the simple two-dimensional shear flow described in Figure 2a does not describe the flow field in the retracting drop adequately, but one should consider the unsteady boundary layer flow on the target surface, with a shear velocity gradient that can be approximated as:

$$u_y \approx \left( \frac{\partial u}{\partial y} \right)_{y=0} \approx \frac{2U(x)}{h(x)} \quad (4)$$

167 where  $U(x)$  and  $h(x)$  are the instantaneous free stream velocity in the radial direction  
 168 and the boundary layer thickness at a distance  $x$  from the contact point, respectively.

169 Since the fluid is radially flowing back towards the drop centre, conservation of  
 170 mass implies that in the first stages of recoil the velocity magnitude increases, so that  
 171  $v_x > 0$ . Thus, the ratio between the anti-symmetric and the symmetric part of the  
 172 velocity gradient tensor is smaller than unity, which triggers the second-order coil-  
 173 stretch transition as discussed above [15,23]. Moreover, in a boundary layer  $u_y \gg v_x$ ,  
 174 therefore the polymer molecule fractional stretching given by Eq. (1) does not depend  
 175 significantly on the radial velocity gradient of the vertical velocity component,  $v_x$ .



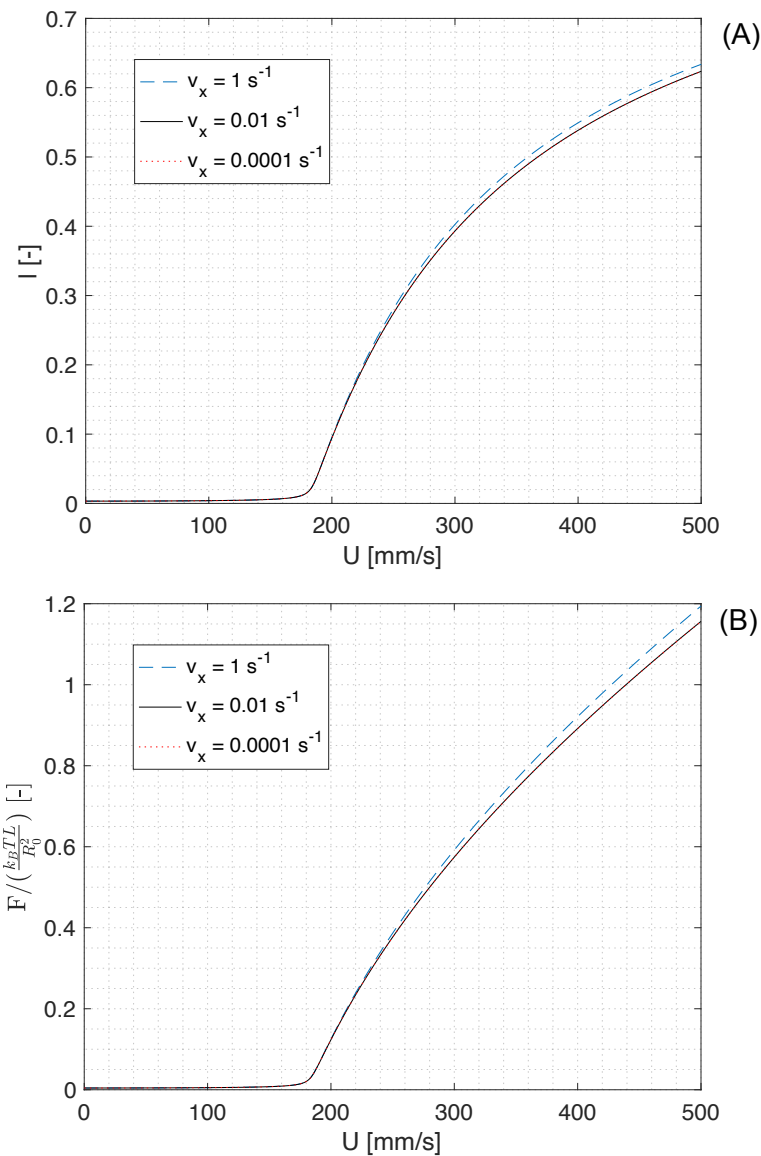


**Figure 4.** Polymer fractional elongation (a) and dimensionless recall force (b) as a function of shear velocity  $U$ , for a shear layer thickness  $h \approx 0.2 \mu\text{m}$  and different magnitudes of the radial velocity gradient  $v_x$ .

176 The numerical solution of Eq. (1) for a boundary layer of thickness  $h \approx 0.2 \mu\text{m}$   
 177 (i.e., just above the polymer coil size  $R_0$ ), and the corresponding recall force of a single  
 178 polymer molecule (Eq. 3) are displayed in Figures 4a and 4b, respectively. These  
 179 figures suggest that, irrespective of the magnitude of the gradient of the vertical velocity  
 180 component  $v_x$ , an appreciable stretching of polymer molecules and consequently a  
 181 buildup of the recall force occur for velocities  $U \gtrsim 200$  mm/s. Since the radial velocity in  
 182 the lamella is of the order of 300 mm/s [8], and the velocity of the fluid in the rim is even  
 183 faster as the rim flows over the lamella during recoil (see Figure 3b), one can conclude  
 184 the shear flow near the contact line of the recoiling drop is sufficient to trigger the  
 185 supercritical coil-stretch transition and cause a large deformation of polymer molecules,  
 186 which can reach a mean fractional extension  $l \approx 0.5$ .

187 These results are confirmed both qualitatively and quantitatively by the work of  
 188 Smith et al. [26], who directly observed the conformational dynamics of individual,  
 189 flexible polymers in steady shear flow by the use of video fluorescence microscopy. In  
 190 particular, it was found polymers reach an asymptotic mean fractional extension  $l \approx 0.5$ ,

191 characterised by a practically flat probability density between  $l \approx 0.1$  and  $l \approx 0.7$  [26];  
 192 this is also consistent with the direct observation of stretched DNA molecules [7] and of  
 193 thin liquid filaments behind the receding contact line (Figure 1).

Thus, at the beginning of drop recoil, which occurs when the contact angle is still  $> 90^\circ$ , the partially stretched polymer molecules on the de-wetted substrate induce a recall force on the receding contact line, opposed to the contact line velocity; this can be interpreted, from a macroscopic point of view, as an additional, dissipative force acting on the contact line and opposed to its movement, or an effective contact line friction. Figure 5 displays a schematic of the contact line forces in case of a drop of a pure fluid (Figure 5a) and in case of a dilute polymer solution (Figure 5b). Since the drop-surface system is not at thermodynamic equilibrium, the Young-Laplace equation  $\gamma_{SV} = \gamma_{SL} + \gamma_{LV} \cos \theta$  (where  $\gamma_{SV}$ ,  $\gamma_{SL}$  and  $\gamma_{LV}$  are the solid-vapour, solid-liquid, and liquid-vapour interfacial tensions, respectively, and  $\theta$  is the equilibrium contact angle) is not applicable. However, the contact line displacement is driven by surface forces, therefore one can write the following inequality:

$$\gamma_{SL} + \gamma_{LV} \cos \theta_{app} > \gamma_{SV} \quad (5)$$

194 where  $\theta_{app}$  is the apparent contact angle observed during drop retraction.

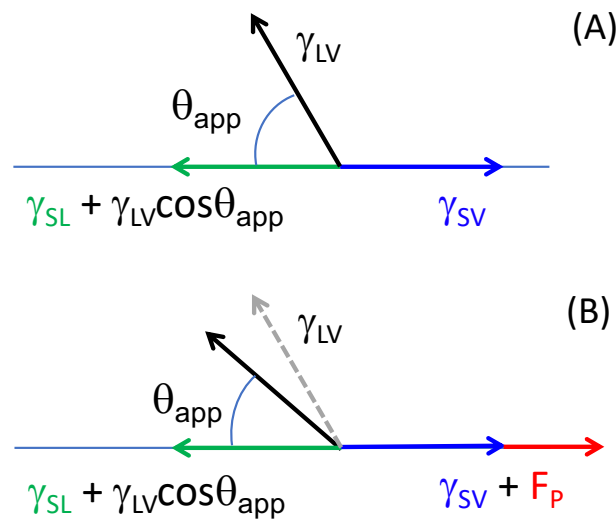


**Figure 5.** Forces acting on the receding contact line for a drop of a pure fluid (a) and for a drop of a dilute polymer solution (b).

In other words, the net force on the contact line in the radial direction determines whether the drop spreads ( $\gamma_{SV} > \gamma_{SL} + \gamma_{LV} \cos \theta$ ) or recoils ( $\gamma_{SV} < \gamma_{SL} + \gamma_{LV} \cos \theta$ ), as shown schematically in Figure 5a. In the case of polymer solutions (Figure 5b), during drop recoil there is an additional resistive force due to the polymer chains stretching,  $F_P$ , so that the condition for recoil becomes:

$$\gamma_{SL} + \gamma_{LV} \cos \theta_{app} > \gamma_{SV} + F_P \quad (6)$$

195 If the magnitude of the polymer force (per unit length of the contact line) is comparable  
 196 to the liquid surface tension,  $\gamma_{LV}$ , the additional resistive force on the contact line is  
 197 compensated by a significant reduction of the apparent contact angle, which is precisely  
 198 what one can observe experimentally ([6,27]).

199 In order to estimate the magnitude of the polymer force per unit length of the  
 200 contact line, one can evaluate an average value of the recall force of a single polymer  
 201 molecule, given by Eq. (3), and multiply it by the number of stretched molecules in a  
 202 vertical liquid wedge near the contact line.



203 Figure 4a suggests that for the measured fluid velocity during recoil [7,8] the  
 204 fractional stretching of polymer molecules is approximately 50%, and the same value can  
 205 be estimated on the basis of the direct observation of the conformational dynamics of  
 206 individual polymers in steady shear flow [26]. The corresponding value of the inverse  
 207 Langevin function is  $\mathcal{L}^{-1}(0.5) \approx 1.8$ .

208 The bulk number density of polymer coils in the fluid wedge is  $n = \rho_p c' N_A / M$ ,  
 209 where  $\rho_p$  is the polymer density,  $N_A$  Avogadro's number,  $c'$  the volume concentration of  
 210 the polymer, and  $M$  its molecular mass. However, the polymer coils that are stretched  
 211 as the contact line sweeps the substrate align in a thin layer at the bottom of the fluid  
 212 wedge, therefore their number scales as  $\approx \sqrt{n}$ .

In conclusion, the overall average polymer force per unit contact line length is given  
 by:

$$F_p = 1.8 \times \sqrt{n} \frac{k_B T L}{R_0^2} \quad (7)$$

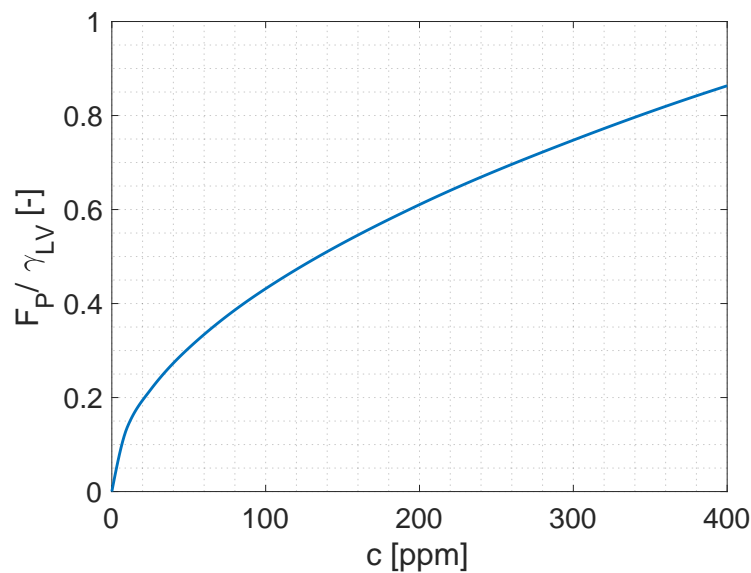


Figure 6. Average polymer stretching force per unit length (Eq. 7), normalized with respect to the surface tension of the solution ( $\gamma_{LV} \approx 70$  mN/m [2,19]), plotted as a function of the polymer mass concentration.

213 Figure 6 shows that the average polymer force per unit length, calculated using  
 214 Eq.(7) for polymer concentrations corresponding to dilute solutions, is comparable in  
 215 magnitude with the surface tension of the polymer solution, therefore it can explain the  
 216 reduction of the contact line retraction velocity observed experimentally. We note the  
 217 force given by Eq. (7) cannot be used directly as an additional term in a Young-Laplace  
 218 force balance because the system is very far from equilibrium, therefore the apparent  
 219 contact angle is not thermodynamically significant. However, the proposed approach  
 220 provides a quantitative explanation of the phenomenon from first principles without any  
 221 empirical parameters, and without the need to introduce fictitious elongational flows or  
 222 other artefacts.

## 223 5. Conclusions

224 The receding contact line of dilute polymer solution drops after impact on a hy-  
 225 drophobic solid surface exhibits a peculiar morphology, consisting of transient micro-  
 226 scopic dendritic structures generated by the receding contact line, which evolve in a  
 227 similar fashion to the well-known beads-on-a-string mechanism, although in this case  
 228 the observed liquid filaments are stretched due to a shear flow instead of a purely

229 elongational flow. These structures indicate the radial flow in the recoiling drop in-  
230 duces a supercritical coil-stretch transition in the polymer molecules, and consequently  
231 the contact line is subjected to an additional dissipative force opposing its receding  
232 movement.

233 The magnitude of this dissipative force can be estimated using the classical finite  
234 extensibility approach, and is comparable to the magnitude of the surface forces that  
235 cause the drop recoil. The proposed approach provides a quantitative explanation of the  
236 phenomenon from first principles without any empirical parameters, and without the  
237 need to introduce fictitious elongational flows or other artefacts.

238 **Supplementary Materials:** The following are available online at [https://www.mdpi.com/article/](https://www.mdpi.com/article/10.3390/colloids1010000/s_videos)  
239 [10.3390/colloids1010000/s\\_videos](https://www.mdpi.com/article/10.3390/colloids1010000/s_videos). Video S1: Detail of the receding contact line of a pure water  
240 drop after impact on a fluorinated surface. Video S2: Detail of the receding contact line of a 40  
241 ppm PEO solution drop after impact on a fluorinated surface. Video S3: Detail of the receding  
242 contact line of a 60 ppm PEO solution drop after impact on a fluorinated surface. Video S4: Detail  
243 of the receding contact line of a 100 ppm PEO solution drop after impact on a fluorinated surface.  
244 Video S5: Detail of the receding contact line of a 200 ppm PEO solution drop after impact on a  
245 fluorinated surface.

246 **Funding:** This research received no external funding.

247 **Institutional Review Board Statement:** Not applicable.

248 **Informed Consent Statement:** Not applicable.

249 **Data Availability Statement:** Original videos available as supplementary material.

250 **Conflicts of Interest:** The author declares no conflict of interest.

## References

1. Bergeron, V.; Bonn, D.; Martin, J.; Vovelle, L. Controlling droplet deposition with polymer additives. *Nature* **2000**, *405*, 772–5. doi:10.1038/35015525.
2. Crooks, R.; Cooper-White, J.; Boger, D. The role of dynamic surface tension and elasticity on the dynamics of drop impact. *Chemical Engineering Science* **2001**, *56*, 5575–5592. doi:10.1016/S0009-2509(01)00175-0.
3. Bartolo, D.; Boudadoud, A.; Narcy, G.; Bonn, D. Dynamics of non-Newtonian droplets. *Physical review letters* **2007**, *99*, 174502.
4. Rozhkov, A.; Prunet-Foch, B.; Vignes-Adler, M. Impact of water drops on small targets. *Physics of Fluids* **2002**, *14*, 3485. doi:10.1063/1.1502663.
5. Bertola, V. An experimental study of bouncing Leidenfrost drops: comparison between Newtonian and viscoelastic liquids. *International Journal of Heat and Mass Transfer* **2009**, *52*, 1786–1793.
6. Bertola, V. Effect of polymer additives on the apparent dynamic contact angle of impacting drops. *Colloids and Surfaces A: Physicochemical and Engineering Aspects* **2010**, *363*, 135–140. doi:10.1016/j.colsurfa.2010.04.031.
7. Smith, M.; Bertola, V. Effect of polymer additives on the wetting of impacting droplets. *Physical Review Letters* **2010**, *104*, 154502. doi:10.1103/PhysRevLett.104.154502.
8. Smith, M.; Bertola, V. Particle velocimetry inside Newtonian and non-Newtonian droplets impacting a hydrophobic surface. *Experiments in Fluids* **2011**, *50*, 1385–1391. doi:10.1007/s00348-010-0998-6.
9. Bertola, V. Dynamic wetting of dilute polymer solutions : The case of impacting droplets. *Advances in colloid and interface science* **2013**, *193-194*, 1–11. doi:10.1016/j.cis.2013.03.001.
10. Smith, M.I.; Sharp, J.S. Origin of Contact Line Forces during the Retraction of Dilute Polymer Solution Drops. *Langmuir* **2014**, *30*, 5455–5459. doi:10.1021/la5005159.
11. Oliveira, M.; Yeh, R.; McKinley, G. Iterated stretching, extensional rheology and formation of beads-on-a-string structures in polymer solutions. *Journal of Non-Newtonian Fluid Mechanics* **2006**, *137*, 137 – 148. Extensional Flow, doi:https://doi.org/10.1016/j.jnnfm.2006.01.001.
12. Cachile, M.; Cazabat, A.M. Spontaneous Spreading of Surfactant Solutions on Hydrophilic Surfaces:  $C_nE_m$  in Ethylene and Diethylene Glycol. *Langmuir* **1999**, *15*, 1515–1521. doi:10.1021/la980840f.
13. Liu, G.; Zhang, C.; Zhao, J.; Zhu, Y. Study of the Morphology of the Three-Phase Contact Line and Its Evolution by Morphological Examination after Droplet Evaporation of Aqueous Polymer Solutions. *Langmuir* **2008**, *24*, 7923–7930. PMID: 18582133, doi:10.1021/la800452w.
14. Hadj-Achour, M.; Brutin, D. Fractal pattern formation in nanosuspension sessile droplets via evaporation-spreading on a glass substrate. *Colloids and Interface Science Communications* **2014**, *1*, 43 – 46. doi:https://doi.org/10.1016/j.colcom.2014.06.007.
15. de Gennes, P.G. Coil-stretch transition of dilute flexible polymers under ultrahigh velocity gradients. *The Journal of Chemical Physics* **1974**, *60*, 5030. doi:10.1063/1.1681018.

16. Bertola, V. Effect of polymer concentration on the dynamics of dilute polymer solution drops impacting on heated surfaces in the Leidenfrost regime. *Experimental Thermal and Fluid Science* **2014**, *52*, 259–269.
17. Bailey, F.E.; Koleske, J.V. *Poly(ethylene oxide)*; Academic Press: New York, 1976.
18. Kalashnikov, V.N.; Askarov, A.N. Relaxation time of elastic stresses in liquids with small additions of soluble polymers of high molecular weights. *Journal of Engineering Physics* **1989**, *57*, 874–878. doi:10.1007/BF00871770.
19. Glass, J.E. Adsorption Characteristics of Water-Soluble Polymers. II Poly(ethylene oxide) at the Aqueous-Air Interface. *J. Phys. Chem.* **1968**, *72*, 4459–4467.
20. Eggers, J. Nonlinear dynamics and breakup of free-surface flows. *Rev. Mod. Phys.* **1997**, *69*, 865–930.
21. Eggers, J.; Villermaux, E. Physics of liquid jets **2008**. *71*, 036601. doi:10.1088/0034-4885/71/3/036601.
22. Brandrup, J.; Immergut, E.H.; Grulke, E.A.; Abe, A.; Bloch, D.R. *Polymer Handbook (4th Edition)*; John Wiley & Sons, 2005.
23. Lumley, J. Drag reduction in turbulent flow by polymer additives. *Journal of Polymer Science: Macromolecular Reviews* **1973**, *7*, 263–290. doi:10.1002/pol.1973.230070104.
24. Peterlin, A. Hydrodynamics of linear macromolecules. *Pure and Applied Chemistry* **1966**, *12*, 563–586. doi:10.1351/pac196612010563.
25. Kroger, M. Simple, admissible, and accurate approximants of the inverse Langevin and Brillouin functions, relevant for strong polymer deformations and flows. *Journal of Non-Newtonian Fluid Mechanics* **2015**, *223*, 77–87. doi:https://doi.org/10.1016/j.jnnfm.2015.05.00
26. Smith, D.E.; Babcock, H.P.; Chu, S. Single-Polymer Dynamics in Steady Shear Flow. *Science* **1999**, *283*, 1724–1727. doi:10.1126/science.283.5408.1724.
27. Bertola, V.; Wang, M. Dynamic contact angle of dilute polymer solution drops impacting on a hydrophobic surface. *Colloids and Surfaces A: Physicochemical and Engineering Aspects* **2015**, *481*, 600–608. doi:10.1016/j.colsurfa.2015.05.052.